ՀՀ ԿՐԹՈՒԹՅԱՆ, ԳԻՏՈՒԹՅԱՆ, ՄՇԱԿՈՒՅԹԻ ԵՎ ՍՊՈՐՏԻ ՆԱԽԱՐԱՐՈՒԹՅՈՒՆ
ԵՐԵՎԱՆԻ ՊԵՏԱԿԱՆ ՀԱՄԱԼՍԱՐԱՆ

ՊԵՏՐՈՍՅԱՆ ՊԵՏՐՈՍ ԱՐՄԵՆԱԿԻ

ՄԵՏԱՂԱԿԱՆ ՆԱՆՈՄԱՍՆԻԿՆԵՐԻ ՀԱՄԱԿԱՐԳԵՐՈՒՄ ՈՐՈՇ ՊԼԱԶՄՈՆԱՅԻՆ ԵՐԵՎՈՒՅԹՆԵՐԻ ՈՒՍՈՒՄՆԱՍԻՐՈՒԹՅՈՒՆԸ

Ա.04.21 - «Լազերային ֆիզիկա» մասնագիտությամբ
Ֆիզիկա-մաթեմատիկական գիտությունների թեկնածուի
գիտական աստիճանի հայցման ատենախոսության

ՍԵՂՄԱԳԻՐ

ԵՐԵՎԱՆ - 2024

THE MINISTRY OF EDUCATION, SCIENCE, CULTURE AND SPORT OF THE REPUBLIC OF ARMENIA
YEREVAN STATE UNIVERSITY

PETROS PETROSYAN

INVESTIGATION OF SOME PLASMONIC EFFECTS IN THE COMPLEXES OF METALLIC NANOPARTICLES

Thesis for the degree of Candidate of Physical and Mathematical Sciences
Speciality A.04.21 – "Laser Physics"

ABSTRACT

YEREVAN – 2024

Ատենախոսության թեման հաստատվել է Երևանի պետական համալսարանում

Գիտական ղեկավար՝ ֆիզ.-մաթ. գիտ. դոկտոր, պրոֆեսոր Ռ.Բ. Ալավերդյան
Պաշտոնական ընդդիմախոսներ՝ ֆիզ.-մաթ. գիտ. դոկտոր, պրոֆեսոր Ա. Ա. Սահարյան
ֆիզ.-մաթ. գիտ. դոկտոր, Ժ. Ս. Գևորգյան
Առաջատար կազմակերպություն՝ ՀՀ ԳԱԱ Ֆիզիկական հետազոտությունների ինստիտուտ

Ատենախոսության պաշտպանությունը կայանալու է 2025թ. Հունվարի 31-ին ժամը 12:00-ին Երևանի պետական համալսարանում գործող Ֆիզիկայի 049 Մասնագիտական խորհրդի նիստում:

Հասցե՝ 0025 Երևան, Ալեք Մանուկյան փ. 1, ԵՊՀ:
Ատենախոսությանը կարելի է ծանոթանալ ԵՊՀ գրադարանում:
Սեղմագիրն առաքված է 2024թ. Դեկտեմբերի 27:

Մասնագիտական խորհրդի գիտական քարտուղար՝ ֆիզ.-մաթ. գիտ. թեկնածու Վ. Պ. Քալանթարյան

The thesis theme is approved at the Yerevan State University.

Scientific supervisor: Doctor of Phys. Math. Sciences, Prof. R.B.Alahverdyan
Official opponents: Doctor of Phys. Math. Sciences, Prof. A. A. Saharian
Doctor of Phys. Math. Sciences, Z. S. Gevorgyan

Leading organization: The Institute for physical research of NAS RA

The defence of the thesis will take place at 12:00 on January 31, 2024, during the session of the Specialized Council 049 of Physics at the Yerevan State University.

Address: 1 Alex Manoogian Street, 0025 Yerevan, Armenia.
The thesis is available in the Yerevan State University library.
The abstract was distributed on 27 December, 2024.

Scientific secretary of the Specialized Council — Candidate of Phys. Math. Sciences V. P. Kalantaryan

GENERAL DESCRIPTION OF THE WORK

Relevance of the topic. Since its initial discovery and elucidation in investigations of ionization of atomic systems in 1961, Fano resonance (FR) [1] has gathered substantial attention across diverse scientific and engineering disciplines, encompassing atomic physics, electric circuits, photonics, plasmonic structures, and nonlinear optics. This universal interest can be attributed to the intriguing and distinctive line-shape profile exhibited by FR. The ultrasharp and asymmetric spectral features of FRs in optical systems, such as metal-insulator-metal (MIM) waveguides, photonic crystals, metallic metamaterials, and Kerr nonlinear structures, have been involved to realize numerous contemporary optical functionalities. These applications encompass optical switches, diodes, filters, absorbers, and modulators, and have a remarkable performance in sensing technology. Given the extensive array of applications, the precise control of the Fano line-shape profile including both the spectral position and the degree of asymmetry has emerged as a pressing concern and become a prominent research focus in recent years since they directly relate to the application performance. In general, the degree of Fano asymmetry is closely linked to the symmetry of the structure and the discrete state mode. In many cases, breaking the structural symmetry can lead to increased line-shape asymmetry or the emergence of new FRs. In recent years, FR generated in plasmonic nanostructures has gained increasing attention owing to its promising applications in sensing, lasing, switching, nonlinear and slow-light devices. Symmetry breaking represents one way to achieve geometrical, compositional, and environmental dielectric asymmetry in plasmonic nanostructures, which often results in FR. Optical cavities, normally Fabry–Pérot (FP) cavities, provide an alternative way to realize FRs.

Until now, various plasmonic nanostructures, such as metal-insulator-metal waveguide-coupled cavity systems, ring–disk cavities, oligomer clusters, have been experimentally and/or theoretically demonstrated to show FRs. Specifically, plasmonic structures supporting FR can be arrangements of three slabs, or rods in dolmen-like or H-like configuration. In the dolmen-like structure composed of relatively large slab particles, FR appears due to coherent coupling between superradiant and subradiant plasmon modes, that were studied theoretically and observed experimentally. FRs may occur in this case due to the strong transversal-longitudinal coupling as the sizes of the slab components of the structure increase and retardation effects become significant.

The investigation of FR peculiarities as well as its different applications described above relate to nanostructures of regular metals. So far however, the FR was not investigated in new classes of low dimensional materials obeying metallic conductivity synthesized in recent years. Particularly in MXenes discovered in 2011 [2] the FR peculiarities were not considered. Transition metal carbides/nitrides, called MXenes has become the subject of versatile intensive studies due to their unique optoelectronic properties as well as hydrophilicity, flexibility and metal-like electronic conductivity. This interest in MXenes is fueled by the possibility of applications as supercapacitors and in electromagnetic interference shielding, as well as in optical sensing and light detection, even in communication and biology. The study of the optical properties of MXenes showed the possibility of creating transparent conductive electrodes, saturable absorbers for femtosecond mode-locked lasers, for photonic devices and for plasmonic applications at wavelengths. MXenes reported to date are synthesized by wet-chemical etching

in hydrofluoric acid (HF) or HF-containing or HF-forming etchants. Etching is required because of strong chemical bonds between A and M elements in MAX phases that make mechanical exfoliation hardly possible. To date, more than 50 members of the MXene family have been synthesized [3] and dozens more are predicted, making it one of the fastest growing 2D material family.

· **The aim of the thesis** is to study the conditions of appearance of FR in optical absorption processes and SERS in complexes of MXene NPs.
The following problems are considered.

- Investigation of absorption cross-section (ACS) in isolated and coupled (dimers) MXene NPs of different shapes and comparison with experiments
- Calculation of enhancement factor (EF) of SERS from dye molecule near the MXene nanoparticles (NPs) of various shapes and comparison with known experiments
- Calculation of SERS EF from dye molecule located in the middle of the gap of MXene dimer under the conditions of FR
- Revealing FR in coupled identical spheroidal metallic particles in a symmetric linear arrangement
- Investigation of the influence of retardation and radiation reaction on FR efficiency
- Investigation of FR in 3D system of metallic NSs

Scientific novelty. In contrast to noble metals MXene NPs as the experiments and calculations show, do not demonstrate dipole SP resonances in visible range [4]. This could be interpreted as the unsuitability of these new 2D structures for using them in optical devices, as well as for synthesizing SERS substrates. However, in the thesis we show for the first time that in the visible and near infrared (NIR) range of the spectrum there appear quadrupole SP resonance that along with interband transitions (IBT) is able to induce relatively high polarization of MXene NPs making them attractive for various optical applications. The mechanism of arising of these collective oscillations of quadrupole symmetry is identified as a consequence of inclined incidence of light on ruff surface. As an example of simplest model producing a roughness of NP surface a spheroidal shape is considered. The other new result obtained is that quadrupole surface plasmon (QSP) mode in vis-NIR range in most studded MXene – $Ti_3C_2T_x$ is insensitive to nanoparticle shape and size of NPs. This disclosure opens the perspectives for using MXenes as easy synthesized SERS substrates. Since polarization mechanisms are much less sensitive to the shape of NPs, it can be concluded that despite the fact that MXene substrates demonstrate moderate enhancements as compared to noble metal counterparts, they can provide advantages in conventional SERS applications. The EF values present a weak dependence on the particle shape and size and therefore, there is no need to control the geometry of flakes during their synthesis. This is why MXene flakes can be advantageous for the easy manufacturing of universal substrates for SERS applications.

For the calculation of EF of SERS using COMSOL software it is required to introduce the dielectric functions of both MXene substrate and dye molecule. While the dielectric function of $Ti_3C_2T_x$ MXene is well known, the dielectric function of probe molecule must be introduced. We show that the R6G molecule in different media can be modelled as a small sphere possessing

a macroscopic dielectric function $\varepsilon_R(\omega)$. To obtain $\varepsilon_R(\omega)$ of a small sphere with radius R, as an auxiliary parameter, the imaginary part of polarizability $\alpha_R(\lambda)$ of the dye molecule on glass substrate, or in aqueous solution, is extracted from experimental data of the absorption spectrum [5]. The real part of the dielectric function is calculated using the Kramers-Kronig relation. Namely, $\varepsilon_R(\omega)$ of R6G molecule constructed in the described above way is employed in all simulations.

It is shown that FR appears in MXene dimmers of NSs when the longer axis and aspect ratio (AR) exceeds correspondingly 1 μm and 2.5. It is demonstrated that emergence of FR for the high enough concentrations of MXene NPs on glass or in water can play a role of a measure of good quality of the system as a SERS substrate.

Usually to realize FR in nanoscale the interacting particles are of different shapes, or sizes in order to allow a spectral overlap between their distinct plasmonic modes. We show that when two identical in size spheroidal particles, aligned along their longitudinal symmetry axis, are excited by a plane wave polarized parallel to the axis, both quadrupole modes are excited simultaneously, resulting in a small, but perceptible extinction peak.

Practical importance. The obtained in the thesis results can be used in improving the parameters of already existing devices based on MXenes. Particularly obtained in the thesis result on insensitivity of QSP mode to nanoparticle shape and size in most studded MXene – $Ti_3C_2T_x$ will be used in constructing devices for EM shielding.

The revealed in the thesis weak dependence of EF of SERS on sizes of easily synthesized and almost arbitrary shaped MXene NPs in vis-NIR range opens up new possibilities for using these substrates in conventional SERS applications.

Appearance of FR in MXene dimmers will be used for preparing quality SERS substrates.

Identification of main mechanisms of optical absorption of light in vis-NIR range of the spectrum caused by IBT and QSPs mechanisms will support in designing based on MXenes new optical devices for various applications, such as optical filters, sensors for biophysics etc.

The basic results to be defended are as follows:

1. The absorption spectrum of isolated $Ti_3C_2T_x$ MXene in vis-NIR range is formed by IBT, QSP and TDSP resonances. In case of coupled MXene nanoparticles along with mentioned resonances there appears FR.
2. It is demonstrated that QSP modes in MXene flakes supported by IBT contribute to the SERS enhancement for wavelengths $\lambda \leqslant 1000\, nm$. Raman signal enhancements of the order of $10^5 - 10^7$ obtained in the simulations and agreeing well with known experimental data are determined by the partial overlapping of the QSP, IBT, and analyte molecule absorption resonances, as well as by extra enhancement due to the hot-spot effect. The EF of SERS from dye molecule near the MXene substrate weakly depends on linear dimension and shape of synthesized NPs of common sizes $(1 \div 2\, \mu m)$.
3. At $\lambda \sim 1400\, nm$ in coupled MXene NPs acting as a SERS substrate, the hybridization of induced SPs of different symmetry form a FR. This disclosure can be used for assessing the qualities of SERS substrates made from MXene.

4. Retardation effects and reaction field improve the efficiency of FR in interacting relatively small metallic NPs and in case of $Ti_3C_2T_x$ MXene the quadrupole resonance takes place at visible range (750 nm) providing better conditions for SERS.

Approbation of the work. The results of the thesis were reported at the conferences: Materials Research Society Spring Meeting, Honolulu, Hawai'i. USA 2022, META 2022, the 12th International Conference on Metamaterials, Photonic Crystals and Plasmonics" Torremolinos, Spain 2022, Nanometa-2022, the 8th International Topical Meeting on Nanophotonics and Metamaterials, 28 - 31 March 2022, Seefeld, Austria, Biophotonics for future, Jena, Germany, 2023.

Publications. Four papers were published on the topic of the thesis.

Structure of the thesis. The thesis consists of an Introduction, three Chapters, a Conclusion, and a bibliography. It contains 106 pages, including 46 figures.

CONTENT OF THE THESIS

In **Introduction** the scientific literature related to the topic of the thesis is reviewed, the relevance of the topic is argued, the aim of the work, the scientific novelty and the practical value are presented, and the primary results are described.

In **Chapter 1** analyses of experimental data on EEL and optical absorption spectra of $Ti_3C_2T_x$ is presented, that was used to calculate the absorption cross-section (ACS) in isolated MXene nanoparticles of different shapes and compare the results of simulations with experiments. Exploiting the results for ACS of single MXene nanoparticle (NP) the optical properties of dimers of NPs were considered.

Experiments on electron energy loss (EEL) spectroscopy in $Ti_3C_2T_x$, covering a fairly wide range of energies up to 30 eV show that the maxima at lower energy losses 0.2 eV-0.7 eV in stacks of MXenes occur due to longitudinal dipole surface plasmons (LDSPs) [4]. Further, the higher energy losses up to 1.5 eV a weaker maximum was also found, which was revealed in optical spectra of $Ti_3C_2T_x$ as well in [6]. Detected by different methods, this peculiarity has been prescribed to low-energy interband transitions (IBT) [7]. At energies over 5 eV and more, a rather strong IBTs are detected, after which bulk plasmons occur [4]. It was also shown that LDSP frequencies can be tuned in the mid-infrared by controlling the sheet geometries and terminations. Moreover, it was revealed that in multilayered (ML) MXene sheets the individual 2D flakes interact weakly, apparently reducing the intensity of bulk excitations and leaving LDSPs as a source of dominant screening mechanism.

It is important to mention that in some parts of the EEL spectra of experimentally studied ML MXenes, it is difficult to distinguish IBT from TSP by absorption. This is because particularly in $Ti_3C_2T_x$, the peak frequencies of IBT and TSP are located close to each other, and in case of excitation of TSPs, the electric field distribution is not projected on the plane of incident wave (but on the plane perpendicular to that). As for the peak frequency of IBT, it is independent on the geometry of the sample and is determined only by the dielectric properties of the material.

Contrary to EEL spectroscopy experiments, in the case of irradiation by light, these two processes can be identified in absorption experiments by changing the polarization of the radiation.

To consider the objectives of the thesis it was necessary to solve a number of boundary problems of electrodynamics. Out of several numerical approaches based on finite element method (FEM) we apply COMSOL MULTYPHYSICS software package that allowed to simulate all the problems considered in the thesis. The corresponding numerical calculations were performed with the support of the computing center facilities of the University of Ulm.

The numerical simulations on optical spectra of large MXene nanoparticles (up to 2000 nm) exploiting analytically a priori identified ranges of resonance frequencies for various configurations and shapes as presented. The shapes and sizes of NPs (with measured dielectric function [8] were modelled with the aim to be as close as possible to synthesized samples in mentioned above experiments. The resulting spectra for the ACS and the EF are accompanied with corresponding electric charge and near field distribution maps extracted at specific wavelengths. Throughout the thesis in the scale bar on the right side of each inset the absolute values of electric field strength in arbitrary units are presented. In the figures of the paper the Z axis is directed along the wave incidence and the electric field oscillates along the Y axis. Experimental MXene 2D flakes present a large shape variety, depending on the fabrication conditions. Hence, we model several flake shapes to see what kind of shape-dependent peculiar plasmonic effects are also evidenced in experiments. While in the disk with the diameter of 500 nm and height 14 nm there appear only IBT and TDSP oscillations (Fig.1), in the cylinder of diameter of 1000 nm with the height 300 nm there are IBT and QSP (Fig.2)

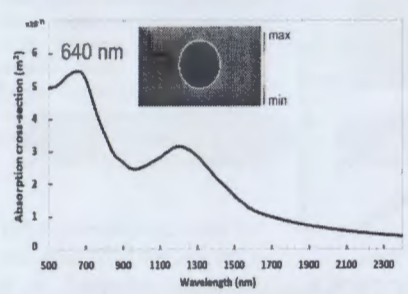

Fig.1 Simulated ACS of a $Ti_3C_2T_x$ disk of 1000 nm diameter with height 14 nm. The incident electric field is perpendicular to the base of the disk

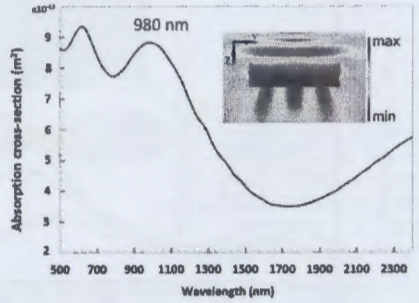

Fig.2 $Ti_3C_2T_x$ cylinder of diameter 1000 nm with height 300 nm. Inset: electric field intensity map wavelength of QSP resonance - 980 nm at the

At $\lambda \sim 1000$ nm the penetration depth d of an incident wave defined as $d^{-1} = (2\pi/\lambda) Im\left(\sqrt{\varepsilon(\lambda)}\right)$ (where λ is the wavelength in the vacuum) takes a value of ~100 nm. Consequently, decrease of electric field amplitude in the direction of propagation can cause inhomogeneity and induce QSP excitations in the plane formed by the directions of wave incidence and electric field.

Indeed because of strong absorption, the energy of incident light is dissipated fully in the narrow surface layer not reaching deeper parts of cylinder. Thanks to inclined incidence on cylindrical surface obviously components of oscillations of electric field in transversal with respect to incident field direction is generated supporting QSP. SP oscillations excited by the transversal components of the electric field (i.e. along the light incidence direction) arise due to the refraction of light at every point of cylinder surface. Calculation of the wavelength λ_m of oscillations induced by the pump wave at 980 nm in the medium determined by the formula $\lambda_m = \lambda/\sqrt{Re(\varepsilon(\lambda))}$ ($\varepsilon(\lambda)$ is the complex dielectric function of MXene) gives for $\lambda_m = 363nm$. Such value of λ_m obviously allows excitation of quadrupole mode in a cylinder with diameter of 1000 nm and a height of 300 nm.

Large and spatially confined electromagnetic enhancement effect can be reached in case of strongly coupled nanoparticles such as dimer configurations. Two closely placed small identical MXene nanoparticles of ellipsoidal or spheroidal shapes in end-to-end configurations were studied for wavelengths range of 500nm-2500nm. To reveal the peculiarities of SP resonances in coupled MXene nanoparticles, we calculate the absorption spectra of two identical interacting spheroidal $Ti_3C_2T_x$ particles in an end-to-end configuration at separations of D=0.8 nm,1 nm and 1.5 nm. The semiaxes of the particles were: a) 20 nm,5 nm,5 nm b) 25nm,5nm,5nm c) 30nm,5nm,5nm) correspondingly. The electric field of the light was directed along the symmetry axis of the system. The results of calculations are presented in the Fig.3.

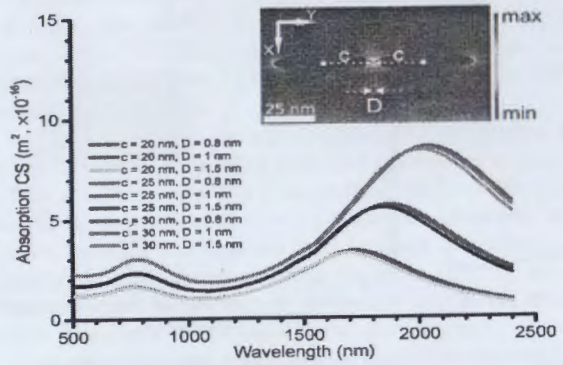

Fig.3 Simulated ACS of coupled MXene nanospheroids in end-to-end configuration with equal short semiaxes ($a = b = 5nm$) and varying long semiaxis ($c = 20, 25\ or\ 30\ nm$). Inset: electric field intensity map in the case of coupled spheroids with semiaxis $c = 25nm$ and $a = b = 5nm$, irradiated by parallel electric field at 760 nm.

It is seen, that contrary to IBT at 750 nm, the LDSP peaks are drastically redshifted. It is interesting that the proposed simple model consisting of coupled ellipsoids gives reasonable value for the SP resonance energy of 0.59 eV- 0.73 eV which was observed in EEL and optical absorption experiments. The corresponding electric field intensity map at 760 nm presented in the inset of Fig. 3 clearly demonstrates the hotspot induced by IBT polarization.

In order to assess the possibility of appearing of QSP resonance in interacting MXene nanoparticles, we also simulated the absorption in notably larger coupled spheroids with semiaxes: 500 nm, 200 nm and 200 nm. The results for the end-to-end configuration of spheroids

when the incident electric field is directed along the long axis are presented in Fig.4. It clearly shows the existence of QSP mode at 980 nm analogous to those revealed for the single cylinder.

Interestingly as can be seen from Fig. 4-A, in addition to quadrupole resonance detected at 980 nm, there is also a new resonance at 1780 nm. We attribute this resonance to longwave quadrupole and transversal plasmon oscillations, the mechanism of occurrence of which differs significantly from the classical one. Typically, the directions of the external field and plasmon oscillations coincide and correspondingly the transversal plasmon oscillations should not occur when the electric field of light oscillates along long axis of coupled spheroids. The point is that the transversal component of electric field is generated in the NS due to inclined incidence of light wave to the spheroidal surface.

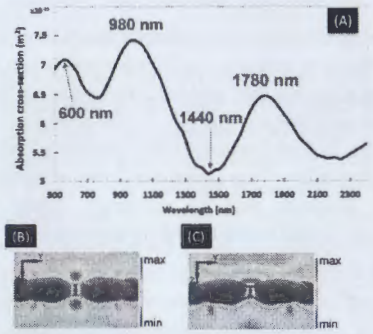

Fig.4 ACS of coupled spheroids with semiaxis 500 nm, 200 nm and 200 nm in end-to-end configuration (A). Electric field intensity maps at TSP maximum - 1780 nm in the X-Y plane (B) and Y-Z plane (C).

It is this (obeying quadrupole symmetry) electric field that creates the charge distribution presented in Fig. 5. In accordance to the Fresnel equations it is clear that any roughness of the surface of NP can generate components of electric field perpendicular to the polarization of incident light. In this respect the model of NS is the simplest case of surface roughness giving rise to transversal oscillations.

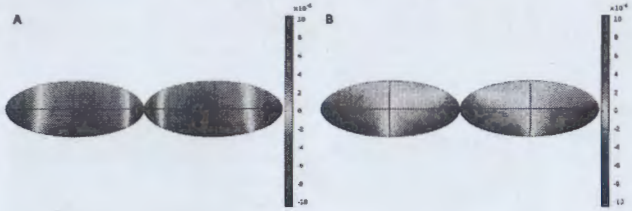

Fig. 5. Surface instant charge distribution for a NS (2a=1000 nm) at 1780 nm (A) for φ=0 and (B) for φ=2.25π where φ is phase of incident field. Red and blue colors represent charges of opposite signs. The areas in gray correspond to zero charge.

It is important to mention, that as a result of strong coupling of QSP and induced TSP modes as it follows from Fig. 4-C there appears a Fano deep at 1440 nm. This lowest minimum at 1440 nm in the spectrum of strongly interacting nanoparticles is a result of destructive interference between QSP and new TSP modes which is a manifestation of FR. In the Fig. 4-C the symmetry of intensity distribution with respect to incident electric field is violated, obviously demonstrating appearance of a QSP resonance. The electric field intensity maps at FR in the XY-plane and YZ-plane are presented in Fig. 6-A and B.

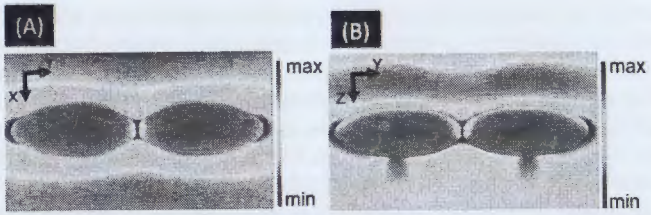

Fig.6 Electric field intensity maps at QSP maximum - 980 nm in the X-Y plane (A) and Y-Z plane (B).

In **Chapter 2**, the SERS EF of the probe molecule near an isolated MXene flake, either in a solution, or on a substrate. Next, to account for the hot spot effect using the same software we perform simulation of ACS and SERS EF for interacting MXene dimers.

To calculate accurately the EF, it is required to introduce the dielectric function of the dye molecule as well. We show that the R6G or other dye molecule in different media can be modelled as a small sphere with radius R possessing a macroscopic dielectric function ε_R (ω). Namely, having measured polarizability $\alpha(\lambda)$ of due molecule we find $\varepsilon_{R6G}(\lambda)$ from employing R as a fitting parameter. The wavelength dependent ACS of dye molecule is calculated using $\varepsilon_{Rh}(\lambda)$ in COMSOL software. Thus, we find the fitting value of the parameter R that achieves a good overlapping between the calculated ACS spectrum and the maximum values of experimental data. The theoretical EF G, is defined according to the following expression:

$$G = \frac{\left|\vec{E}_{total}(\vec{r}_0,\omega)\right|^4}{\left|\vec{E}_0(\vec{r}_0,\omega)\right|^4}. \quad (1)$$

$\vec{E}_{total}(\vec{r}_0,\omega)$ is a total electric field at the position of the probe molecule $\vec{r}_0$, ω is the frequency and $\vec{E}_0(\vec{r}_0,\omega)$ is the strength of the incident field. In the Fig. 7 the simulated EF of SERS from R6G molecule near the apex of single MXene NE with $2a = 500\,nm$ reaching the maximum value of $G \approx 2.21 \cdot 10^5$ is presented.

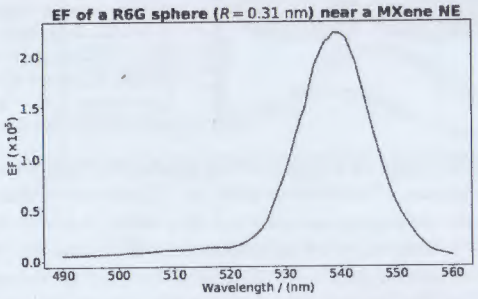

Fig.7 EF of SERS from R6G molecule near the apex of single MXene NE with $2a = 500\,nm$ and aspect ratios $\eta_1 \approx 3$ and $\eta_2 \approx 15$ on glass substrate. The distance from the apex of NE to the dye molecule (presented as a small sphere of radius $R = 0.31\,nm$, see figure SI-1) is $s = 0.4\,nm$.

In order to understand the SERS enhancement mechanisms of molecules near MXene flakes, we use an example presented in Fig. 8. It illustrates the dependence of ACS on wavelength for a NE with $2a = 500\,nm$ and aspect ratios $\eta_1 \approx 3$ and $\eta_2 \approx 15$.

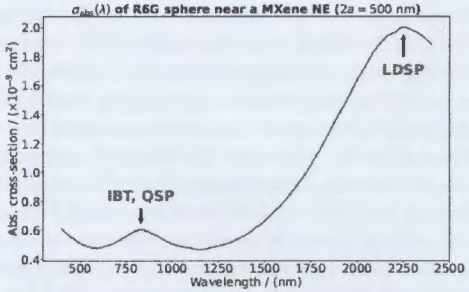

Fig. 8. ACS dependence on wavelength in the system of spherical R6G molecule and MXene NE with $2a = 500\,nm$ and aspect ratios $\eta_1 \approx 3$ and $\eta_2 \approx 15$. The arrows indicate the positions of the longitudinal

From the ACS spectrum of Fig 8, we assume that the highest peak at $\lambda = 2250\,nm$ corresponds to the longitudinal dipole surface plasmon (LDSP) resonance. To support this assumption, we carried out simulations for NEs of $2a = 500\,nm$ but with other aspect ratios. The results revealed high sensitivity of the location of that peak to the shape of NP, which is a typical behavior of longitudinal dipole plasmon oscillations. This sensitive to NP shape resonance was revealed also in high-resolution EELS experiments with $Ti_3C_2T_x$ flakes [2, 3]. The same LDSP resonance at $\lambda > 2200\,nm$ was revealed in [4] using UV-Vis-NIR absorption spectroscopy of micrometer sized $Ti_3C_2T_x$ samples. The smaller peak in the spectral range 500 nm-1000 nm of Fig. 8 coincides with the maximum of absorption (or a dip in the transmittance spectrum) measured in Ti3C2Tx flakes in an aqueous solution, on a glass or sapphire substrates [7-10], as well as in measured EELS spectra [4,11]. In optical absorption measurements, the maximum at around λ=800 nm was associated to IBT, which was theoretically verified in [7]. The physical origin of the peak in the spectral range of $500\,nm - 1000\,nm$ of Fig.8 becomes obvious by visualizing the surface charge and near-field maps of our COMSOL simulation. These maps for the NE of $2a = 500\,nm$, $\eta_1 \approx 3$ and $\eta_2 \approx 15$ at $540\,nm$ (corresponding to the EF maximum) are presented in the Figs 9 a) and b) respectively.

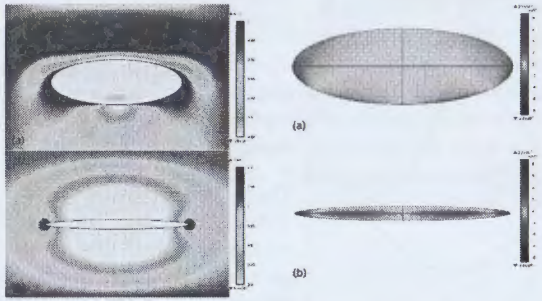

Fig9 a) b) The maps of electric field and instant chart distribution for NE of 2a=500 nm, η_1≈3 and η_2≈15 at 540 nm

These figures clearly demonstrate the quadrupole character of the SP oscillations excited by the transversal components of the electric field (i.e. along the Z axis) arising due to the refraction of light at every point of NE surface. Just in case of cylinder described in Chapter 1, at any pare of points symmetrical with respect to the Z axis of the NE refraction occurs in such a way that the generated transversal components of the electric field have opposite directions. It is this (obeying quadrupole symmetry) transversal

electric field that creates the charge distribution presented in Fig 9 b). Note that in accordance to the Fresnel equations any roughness of the surface of relatively large NPs can generate transversal components of electric field. In this respect the ellipsoidal surface represents the simplest model of surface roughness giving rise to transversal oscillations. Whereas the QSP in MXene at wavelengths $\lambda \leq 1000\ nm$ were identified earlier, we see from Fig. 9a and 9b that in the surface charge distribution instant image there appear also dipole oscillations due to IBT. Therefore, we conclude that at wavelengths $\lambda \leq 1000\ nm$ QSP and IBT resonances both contribute to the absorption peak in Fig 8. This means that in large MXene NPs considered here QSP resonance overlaps with IBT, creating favorable conditions for Raman signal enhancement in vis-NIR spectral range. As our simulation shows in the range $500\ nm - 1000\ nm$ the quadrupole oscillations remain dominant in charge distribution. The resonance maximum occurs at $\lambda = 850\ nm$, but the quadrupole charge distribution remains at $\lambda = 540\ nm$. Simulations were carried out for larger sizes of ellipsoidal flakes ($2a = 1500\ nm$ and $2a = 2000\ nm$) as well. In the spectral range of $\lambda \leq 1000\ nm$ in NEs with aspect ratios $\eta_1 \approx 3$, $\eta_2 \approx 15$, quadrupole and higher order SP modes start to play a more pronounced role in optical absorption processes (see e.g. instant picture of surface charge distribution of MXene NE with $2a = 2000\ nm$ at $540\ nm$ in Fig.10a). Instant charge distribution maps for this particle at other resonances are presented below in Fig.10b.

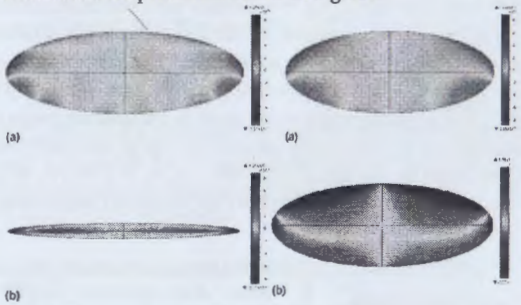

Fig 10 a, b instant picture of surface charge distribution of MXene NE with $2a = 2000\ nm$ at $540\ nm$

Interestingly, in larger particles with $2a = 1500\ nm$ and $2a = 2000\ nm$ and aspect ratios $\eta_1 \approx 3$, $\eta_2 \approx 15$ an additional resonance appears in the ACS spectrum, as is shown in the Fig. 11.

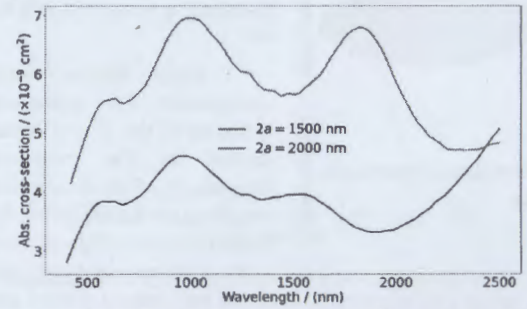

Fig.11 ACS dependence on wavelength in the MXene NE with $2a = 1500\ nm$ (blue) and $2a = 2000\ nm$ (red) (aspect ratios $\eta_1 \approx 3$ and $\eta_2 \approx 15$).

These new resonances arise at $1540\ nm$ and $1830\ nm$ correspondingly. The Instant picture of surface charge distribution clearly show the dominant contribution of quadrupole modes in these resonances. Thus, along with resonances at $\lambda \leq 1000\ nm$ there appear new QSP resonances at much longer wavelengths. We note that our simulations for NSs

of $2a = 1500\ nm$ and $2a = 2000\ nm$ and aspect ratio $\eta \approx 3$ did not reveal QSP oscillations at longer wavelengths. This means that QSPs at longer wavelengths in large oblate NEs are excited by the electric field directed along the shortest axis occurring due to refraction of incident light on the ellipsoidal surface. Note that these new resonances are far from R6G absorption peak and therefor are not important for SERS in vis-NIR range.

Atomic force microscopy (AFM) images of MXene flakes show often bent sheets and curved surfaces with a number of edges supporting the origin of localized strong EM fields. Consequently, MXene flakes deposited on substrate or in solution can provide favorable conditions for another EM mechanism of SERS – hot-spot effect. Dimers of $Ti_3C_2T_x$, in a "end - to - end" configuration composed of identical NEs, NSs and NRs of different sizes on glass substrate with the R6G molecule located in the middle of the gap were investigated. In Figs. 12(a) and 12(b) are presented the ACS and EF for a dimer of identical spheroidal particles of $2a = 1000\ nm$ and aspect ratios $\eta_1 \approx 3$ and $\eta_2 \approx 15$ on the glass substrate.

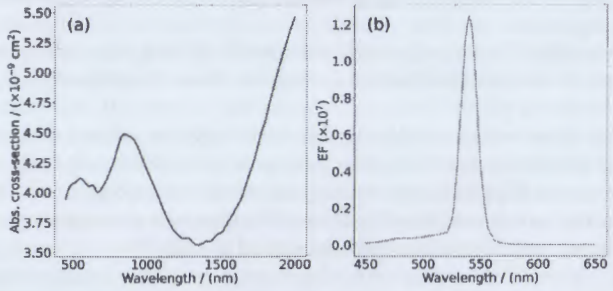

Fig 12 ACS and EF for a dimer of identical spheroidal particles of $2a = 1000\ nm$ and aspect ratios $\eta_1 \approx 3$ and $\eta_2 \approx 15$ on the glass substrate

According to Fig 12(b) the EF in case of dimer due to near-field coupling resulting in hot-spot effect is $1.2 \cdot 10^7$. A notable contribution to the EF in the dimer is due to polarization induced by the resonance absorption of the R6G dye at short wavelength of $545\ nm$ [5].

To assess the dependence of ACS on the gap length in a dimer we calculated the absorption spectra of identical NS particles with sizes $2a = 1000\ nm$ and $2b = 2c = 400\ nm$ in "end-to-end" configuration, with incident field parallel to the symmetry axis of the dimer (see Fig. 13). For wavelengths below $1300\ nm$ the ACS of the dimer does not depend on the gap size since QSP oscillations in both particles weakly interact to each other. At longer wavelengths a new resonance depending on the dimer gap size arises as a result of strong hybridization of quadrupole modes in two NSs. We interpret the minimum in the ACS at $\lambda = 1440\ nm$ of Fig. 13 as a Fano dip formed by coupling between QSP modes in dimer.

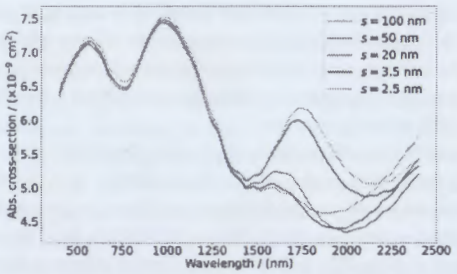

Figure 13. Dependence of ACS on the size of the gap of dimer composed of identical NSs with $2a = 1000\ nm$ and $2b = 2c = 400\ nm$ in "end-to-end" configuration when the incident electric field is parallel to particles longitudinal symmetry axis. The gap values are shown in the inset.

For the case described in Fig.36 the simulation for the EF gives the value $1.24 \cdot 10^7$ and with increase the gap of dimer the EF decreases. Particularly for the gap values $s > 100\ nm$ when the dye molecule is fixed in the center of the gap the EF coincides with that of isolated NE of the same size of $2a = 1000\ nm$. This behavior of ACS at FR dip can be used for synthesizing quality MXene substrates for SERS. Indeed, by adding $Ti_3C_2T_x$ flakes say on glass substrate and controlling the ACS dependence on wavelength it will be easy to get the best quality substrate with highest hot-spot effect.

Chapter 3 considers behavior of FR in complexes of small metallic NPs may when influence of retardation effects, radiation reaction force and broad absorption linewidth on the FR are taken into account.

It is shown, that when two identical in size spheroidal particles, aligned along their longitudinal symmetry axis, are excited by a plane wave polarized parallel to the axis, both quadrupole modes are excited simultaneously, resulting in a small, but perceptible extinction peak. Despite being weaker as it is seen from Fig.14 than the absorption the scattering cross-section presents a resonance with asymmetric lineshape, typical of a FR.

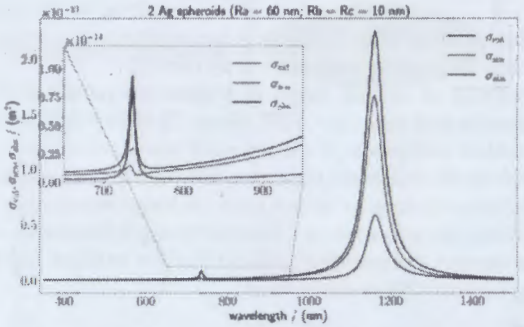

Fig. 14 (Left) Extinction cross-section spectra of two linearly aligned Ag spheroids of semiaxes $ra = 60\ nm, rb = rc = 10\ nm$, separated by $s = 5\ nm$, embedded in a medium of refractive index $n = 1.5$. The large resonance peak close to 1170 nm corresponds to the dipole mode. The inset shows the extinction peak due to coupling of quadrupoles. This wavelength is close to that of the quadrupole resonance arising in a isolated particles.

The FR is considered in the system consisting of five identical smaller than λ metal nanoparticles arranged in one plane in H-like configuration (see Fig.15). The interparticle interaction is taken into account not only by the near field, but also by the fields whose strengths decrease with the distance R as R^{-2} and R^{-1} in contrast to the strength of the dipole near field, decreasing as R^{-3}.

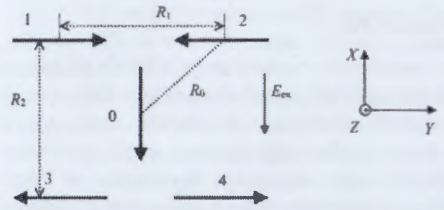

Fig. 15. H-shaped configuration of metallic nanoparticles. The arrows indicate the directions of the spheroid dipole moments for the fixed instant of time.

An external electromagnetic wave will excite oscillations only in the nanoparticle 0, and in other nanoparticles, taking into account their orientation, the longitudinal oscillations will not appear. In the nanoparticle 0, the dipole oscillations will occur, whose frequencies coincide with the frequency of the external field, and therefore, the nanoparticle 0 will create its own dipole field. The frequency of the dipole radiation of the nanoparticle 0 coincides with the longitudinal oscillation frequency of the remaining nanoparticles, and the field generated by the nanoparticle at the locations of nanoparticles 1–4 will have the components along the axes of these nanoparticles; for that reason, the longitudinal oscillations with the frequency of external radiation will be excited in the nanoparticles 1–4.

Thus, each particle creates its own dipole field, which influences all other nanoparticles of the system. Therefore, for example, six fields will influence the nanoparticle 1: the radiation reaction field, the external field and the fields created by the nanoparticles 0, 2, 3 and 4. Owing to the destructive interference of the external field, reaction field and total field of the nanoparticles, the following can arise at a certain frequency of external radiation: the strength of the resulting field at the location of the nanoparticle 0 will become very close to zero, and in other nanoparticles the amplitude of oscillations at this frequency will be much greater than the amplitude of oscillations in particle 0. We further calculate the absorption power of an electromagnetic wave in particles 0 and 1–4 to find the FR efficiency

$$FRE(\omega) = \frac{N_{1234}(\omega)}{N_0(\omega)} \qquad (2).$$

where $N_{1234} = N_1 + N_2 + N_3 + N_4$ is a sum of absorption power in four horizontal NPs and N_0 is a absorption power in vertical NP. It turns out that the FRE is increased by 8 times.

The FR was also studied in a three-dimensional system of identical NSs whose centers are located at the vertices of the tetrahedron (Fig. 16).

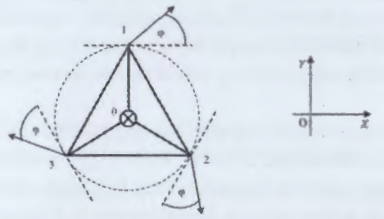

Fig. 16. Oscillatory system consisting of two parts, A and B. The NRs 1, 2, and 3 form the part B, and the NR 0 is the part A. The NR of system B and the tangent to the circumscribed circle of the triangle 123 at the corresponding point form an angle φ.

It is shown that the resonance wavelength of Fano dip is quite flexible and can be shifted by 2.5 times rotating all tree particles in the base around the axes parallel to the 3th order symmetry passing through the upper vertex by 66°. In the same conditions the FRE is increased by 8 times.

CONCLUSIONS

1. Incorporating the experimentally measured dielectric function of Ti3C2Tx MXene and performing simulations of optical absorption spectra of 2D nanosheets we show that the main peculiarities of recently reported electro-optical experiments in vis-NIR range can be reproduced. Moreover, some details of EEL spectra in the range of energy $\sim 1eV$, particularly concerning IBT wavelength range are clarified. The resonance wavelengths of dipole longitudinal and transversal, as well as QSP oscillations in MXene nanosheets of different geometries are identified. The calculated ACSs' resonance wavelengths agree well with experimentally measured once.

It is revealed that the resonance wavelength of the dipole SP mode for large nanoparticles can be tuned down to 1700 nm range. It is shown that rather strong quadrupole mode can be as short as 980 nm. We demonstrate that the plasmonic phenomena in vis-NIR range of the $Ti_3C_2T_x$ MXene occur at the QSP resonance wavelengths, that is at shorter wavelength than that of the transversal one $\lambda \sim 1100\ nm$.

A new mechanism of excitation of TSP oscillations by orthogonal external electric field caused by roughness of the surface of sample is presented. Owing to a strong quadrupole-transversal SP interaction, the possibility of realization of Fano resonance in coupled large spheroidal nanoparticles is demonstrated for the first time, indicating a new direction for exploring additional optical resonance effects in MXenes.

2. SERS EF from R6G molecule near titanium carbide MXene flakes as substates of different size and shape is investigated theoretically in order to interpret known experimental results. To account for the effect of the dye resonance on the EF, we calculate the dielectric function of R6G and MB molecules based on experimental data of the ACS obtained in water or on glass substrate. Since the dielectric function is a macroscopic property necessary to describe the optical materials used in COMSOL, dye molecules are modeled as small solid spheres of polarizability $\alpha(\omega)$, with α extracted from measurements for both of the molecules. This modeling was performed with the COMSOL simulation allowing a simple procedure to choose the proper radius of the small sphere to fit experimental data on absorption by dye molecules. Despite the fact that the polarizability is a tensor, the optical properties are usually averaged over numerous R6G or MB molecules' random orientations. Thus, in interpretation of experiments, the anisotropy of polarizability does not matter. For comparison with experimental data, the same model was performed when analyte molecules are placed near the MXene particle in vacuum.This modelling was performed allowing simple fitting procedure to choose proper radius of small sphere.

3. It was shown that Raman signal EF weakly depends on the shape and size of Ti3C2Tx flakes for wavelengths $\lambda \leq 1000$ nm. It was also demonstrated a crucial role of QSP resonances with MXene substrates. To account for the hot spot effect a coupled MXene NPs in the form of NEs and NSs were considered and the peculiarities following from hybridization of different SP modes are revealed. The results of simulation for MXene substrates in vis-NIR spectral range provide EF values of the order of $10^5 - 10^7$ close to experimental data for Ti3C2Tx.

The weak dependence of EF on sizes of easily synthesized and almost arbitrary shaped MXene NPs in vis-NIR range opens up new possibilities for using these substrates in conventional SERS applications.

At $\lambda \sim 1400\ nm$ in coupled MXene NPs acting as a SERS substrate, the hybridization of induced SPs of different symmetry form a FR acting as a measure of substrate quality.

4. It is shown that QSPs can occur in the complexes of nanoparticles with sizes smaller than the wavelength of incident light. Particularly it was demonstrated that FRE can be controlled by changing the geometry of the system of small metallic NPs. Varying the orientation of individual NPs in the base of the 3D complexes causes change of resonance wavelength of Fano dips. Particularly in case of four NPs forming tetrahedron with tree particles in the base it is possible shifting resonance wavelength of Fano dip by 2.5 times rotating all tree particles in the base around the axes parallel to the 3th order symmetry passing through the upper vertex by 66 °. In the same conditions the FRE is increased by 8 times.

REFERENCES

1. Fano, U., Phyis. Rev. 124, 1866 (1961).
2. Naguib, M., M. Kurtoglu, V. Presser, J. Lu, J. Niu, M. Heon, L. Hultman, Y. Gogotsi, M. Barsoum Advanced Materials 23, 4248–4253 (2011).
3. Yury Gogotsi, Chemistry of Materials 35 (21), 8767-8770 (2023).
4. V. Mauchamp, M. Bugnet, E. Bellido, G. Botton, P. Moreau, D. Magne, M. Naguib, T. Cabioc'h, M. Barsoum Phys. Rev. B 89, 235428 (2014).
5. Djorović, A., Meyer, M., Darby, B. L. & Le Ru, E. C. *ACS Omega* **2**, 1804–1811 (2017).
6. Satheeshkumar, E. T. Makaryan, A. Melikyan, H. Minassian, Y. Gogotsi & M. Yoshimura. Sci Rep **6**, 32049 (2016).
7. A.Sarycheva, T. Makaryan, K. Maleski, E. Satheeshkumar, A. Melikyan, H. Minassian. M. Yoshimura, Y.Gogotsi, JPCC 121, 19983–19988 (2017).
8. A. Dillon, M. Ghidiu, A. Krick, J. Griggs, S. May, Y. Gogotsi, M. Barsoum, A. Fafarman, Adv. Funct. Mater. 26, 4162-4168, 2016.
9. S. Adomavičiūtė, S. Ramanavičius, A. Popov, V. Šablinskas, O. Gogotsi, A. Ramanavičius. Chemosensors 9, (2021).
10. Sarycheva, A. & Gogotsi, Y. Chemistry of Materials 32, 3480–3488 (2020).
11. El-Demellawi, J. K., Lopatin, S., Yin, J., Mohammed, O. F. & Alshareef, H. N. ACS Nano 12, 8485–8493 (2018).

PUBLICATIONS ON THE TOPIC OF THE THESIS

1. Melikyan, A. O., Minasian, H. R. & Petrosyan, P. A. Fano resonance in 3D system of metallic nanoparticles. Journal of Contemporary Physics (Armenian Academy of Sciences) 52, 317–323 (2017).

2. Petrosyan, P. A. Influence of Interaction Retardation and Radiation Reaction on the Fano Resonance Efficiency in the System of Nanoparticles. Journal of Contemporary Physics (Armenian Academy of Sciences) 53, 324–331 (2018).

3. Gonçalves, M. et al. Interband, surface plasmon and fano resonances in titanium carbide (Mxene) nanoparticles in the visible to infrared range. Photonics 8, 1–16 (2021).

4. Minassian, H., Melikyan, A., Goncalves, M. R. & Petrosyan, P. Ti3C2Tx MXene as surface-enhanced Raman scattering substrate. Nanotechnology 35, 415702 (2024).

ԱՄՓՈՓԱԳԻՐ

Ատենախոսությունում տեսականորեն հետազոտված են $Ti_3C_2T_x$ մաքսինի նանոմասնիկների (ՆՄ) օպտիկական հատկությունները և բացահայտված են դրանց զույգերում Ֆանոի ռեզոնանսի առաջացման պայմանները: Ուսումնասիրված է մաքսինի ՆՄ-ի հարևանությամբ տեղադրված ներկայնութի մոլեկուլի կողմից ռամանյան ցրման երևույթը (մակերևույթով ուժեղացված ռամանյան ցրման - ՄՈՒՌՑ): Հաշվարկվել է ՄՈՒՌՑ - ի ուժեղացման գործակցի (ՈՒԳ) կախումը ՆՄ երկրաչափական պարամետրերից, մղման դաշտի ալիքի երկարությաունից, դիմերների դեպքում՝ մասնիկների միջև հեռավորությունից: Բացահայտվել են Ֆանոյի ռեզոնանսի առաջացման պայմանները և այդ ռեզոնանսի դերը որակյալ տակդիրներ պատրաստելու համար:

1. Ներառելով Ti3C2Tx MXene-ի փորձնականորեն չափված դիէլեկտրիկ ֆունկցիան և կատարելով 2D ՆՄ օպտիկական կլանման սպեկտրների հաշվարկներ, մենք ցույց ենք տվել, որ վերջերս այդ նյութերի համար հրապարակված էլեկտրաօպտիկական փորձերի հիմնական առանձնահատկությունները տեսանելի-մերձավոր ինֆրակարմիր տիրույթում կարող են վերարտադրվել: Ավելին, պարզաբանվել են էլեկտրոնի էներգիայի կորուստների սպեկտրոսկոպիայի մեթոդով ստացված սպեկտրների որոշ մանրամասներ՝ 1 ԷՎ էներգիաների տիրույթում: Մասնավորապես բացահայտվել է միջգոտային ռեզոնանսին համապատասխանող ալիքի երկարության տիրույթում կլանման վարքը: Մաքսինի ՆՄ-ում նույնականացվել են փորձով ստացված երկայնական և լայնակի դիպոլային մակերևույթային պլազմոնների (ՄՊ) ինչպես նաև քվադրուպոլ պլազմոնների ալիքի երկարությունները:
2. Բացահայտվել է, որ մեծ նանոմասնիկների համար դիպոլային ՄՊ ռեզոնանսային ալիքի երկարությունը կարող է նվազեցվել մինչև 1700 նմ՝ փոխելով ՆՄ-ի ձևը, ինչը լավ համընկնում է փորձի հետ: Ցույց է տրված, որ բավականին ուժեղ քվադրուպոլ ՄՊ-ի ռեզոնանսային ալիքի երկարությունը կարող է լինել բավականին կարճ՝ 980 նմ: Այսինքն, Ti3C2Tx մաքսինում տեսանելի-մերձավոր ինֆրակարմիր տիրույթում պլազմոնիկ երևույթները տեղի են ունենում քվադրուպոլային ռեզոնանսային ալիքի երկարություններում, այսինքն՝ ավելի կարճ ալիքի երկարությամբ, քան լայնական պլազմոնների դեպքում ($\lambda \sim 1100\ nm$):
3. Ցույց է տրված, որ նմուշի մակերևույթի անհարթություններով պայմանավորված առաջանում է լայնական էլեկտրական դաշտ՝ ծնելով լայնական պլազմոններ: Վերջիններս մաքսինում գրգռում են քվադրուպոլային տատանումներ: Փոխազդող ՆՄ-ի դիմերներում ուժեղ քվադրուպոլ ՄՊ-ը փոխազդելով լայնական պլազմոնների հետ $\lambda \sim 1400\ nm$ առաջացնում է Ֆանոյի ռեզոնանս (դեստրուկտիվ ինտերֆերենցիա): Այս երևույթը հնարավորություն է տալիս հեշտորեն ընտրել որակյալ տակդիրները

ՄՈՒՌՑ-ի համար: Բանն այն է, որ դիմերում ուժեղ փոխազդեցություն հնարավոր է, երբ մասնիկները շատ մոտ են դասավորված իրար նկատմամբ, որի համար անհրաժեշտ է ՆՄ-ների մեծ կոնցենտրացիա:
4. Մաքսինային տակդիրի դեպքում R6G մոլեկուլի ռամանյան ցրման ՈՒԳ հաշվարկվել է կախված ՆՄ-ի չափերից և ձևից, ինչը թույլ է տվել մեկնաբանել հայտնի փորձարարական արդյունքները: Դրա համար նախ և առաջ հաշվարկվել են R6G և MB մոլեկուլների դիէլեկտրիկ ֆունկցիաները՝ հիմնվելով ջրի կամ ապակե հիմքի վրա ներկայութի մոլեկուլի համար ստացված կլանման կտրվածքի փորձարարական տվյալները: Քանի որ դիէլեկտրիկ ֆունկցիան մակրոսկոպիկ հատկություն է, որն անհրաժեշտ է COMSOL-ում օգտագործվող օպտիկական նյութերը նկարագրելու համար, ներկայութերի մոլեկուլները մոդելավորվել են որպես փոքր պինդ գնդիկներ, որոնց բևեռացելիությունը հայտնի է չափումներից: Այս մոդելավորումն իրականացվել է COMSOL-ի թվային հաշվարկի միջոցով, որը թույլ է տալիս պարզ ընթացակարգով ընտրել փոքր գնդիկի շառավիղը՝ ներկայութերի մոլեկուլների կողմից կլանման փորձնական տվյալներին համապատասխանելու համար: Չնայած այն հանգամանքին, որ բևեռացումը թեզոր է, օպտիկական հատկությունները սովորաբար միջինացվում են բազմաթիվ R6G կամ MB մոլեկուլների պատահական կողմնորոշումների վրա: Այսպիսով, փորձերի մեկնաբանության մեջ բևեռացման անիզոտրոպիան նշանակություն չունի:
5. Ցույց է տրվել, որ Ռամանի ազդանշանի ՈՒԳ-ը թույլ է կախված Ti3C2Tx ՆՄ ձևից և չափից $\lambda \leq 1000$ նմ ալիքի երկարությունների համար: Նաև ցույց է տրվել քվադրուպոլային ռեզոնանսների կարևոր դերը մաքսինային տակդիրներում: Թեժ կետի էֆեկտը հաշվի առնելու համար դիտարկվել են զուգակցված մաքսինի նանոէլիպսոիդներ և նանոսֆերոիդներ և բացահայտվել են ՄՊ հիբրիդացումից բխող առանձնահատկությունները: Տեսանելի-մերձավոր ինֆրակարմիր սպեկտրային տիրույթում մաքսինի դիմերներով ապահովում են $10^5 - 10^7$ կարգի ՈՒԳ արժեքներ, որոնք մոտ են Ti3C2Tx-ի փորձարարական տվյալներին:

ՈՒԳ-ի թույլ կախվածությունը հեշտությամբ սինթեզվող և գրեթե կամայական ձևով մաքսինի ՆՄ-ների չափերից տեսանելի-մերձավոր ինֆրակարմիր տիրույթում նոր հնարավորություններ է բացում այս տակդիրների օգտագործման համար՝ սովորական ՄՈՒՌՑ կիրառություններում:
6. Ցույց է տրված, որ QSP-ները կարող են առաջանալ փոքր նանոմասնիկների համալիրներում, որոնց չափերը փոքր են, քան ընկնող լույսի ալիքի երկարությունը: Մասնավորապես, ցույց է տրվել, որ Ֆանոյի ռեզոնանսի արդյունատվությունը կարելի է կառավարել փոքր մետաղական ՆՄ-ների համակարգի երկրաչափությունը փոխելով: Եռաչափ կոմպլեքսների հիմքում առանձին ՆՄ-ների կողմնորոշման փոփոխությունը հանգեցնում է Ֆանոյի ռեզոնանսային ալիքի երկարության փոփոխությանը: Հատկապես այն դեպքում, երբ մասնիկների համակարգը դասավորված է թեթրաեդրոնի գագաթներում, հնարավոր է Ֆանոյի ռեզոնանսային ալիքի երկարությունը փոխել 2,5 անգամ՝ պտտելով հիմքում գտնվող բոլոր մասնիկները վերին գագաթով անցնող 3-րդ կարգի համաչափությանը զուգահեռ առանցքների շուրջը 66°-ով: Նույն պայմաններում Ֆանոյի ռեզոնանսի արդյունատվությունը ավելանում է 8 անգամ:

ПЕТРОСЯН ПЕТРОС

ИЗУЧЕНИЕ НЕКОТОРЫХ ПЛАЗМОННЫХ ЯВЛЕНИЙ В СИСТЕМАХ МЕТАЛЛИЧЕСКИХ НАНОЧАСТИЦ

В диссертации теоретически исследованы оптические свойства максинных наночастиц (НЧ) Ti3C2Tx и выявлены условия возникновения резонанса Фано в их парах. Изучено явление комбинационного рассеяния света (поверхностно-усиленное комбинационное рассеяние - ПУКР) на молекуле красителя, помещенной вблизи НЧ максина. Рассчитана зависимость коэффициента усиления (КУ) ПУКР от геометрических параметров НЧ, от длины волны падающего поля, а в случае димеров - от расстояния между частицами. Выявлены условия возникновения резонанса Фано и роль этого резонанса в изготовлении качественных подложек.

1. Используя экспериментально измеренную диэлектрическую функцию Ti3C2Tx максина и выполнив расчеты спектров оптического поглощения НЧ, мы показали, что основные особенности недавно опубликованных электрооптических экспериментов для этих материалов могут быть воспроизведены в видимом и ближнем инфракрасном диапазоне. Кроме того, выяснены некоторые детали спектров, полученных методом спектроскопии энергетических потерь электронов в диапазоне энергий 1 эВ. В частности, обнаружено поведение поглощения в диапазоне длин волн, соответствующем межзонному резонансу. Длины волн экспериментально полученных продольных и поперечных дипольных поверхностных плазмонов (ПП), а также квадрупольных плазмонов были идентифицированы на НЧ Максина.

2. Установлено, что для крупных наночастиц резонансную длину волны дипольного ПП можно уменьшить до 1700 нм за счет изменения формы НЧ, что хорошо согласуется с экспериментом. Показано, что резонансная длина волны достаточно сильного квадрупольного ПП может быть весьма короткой - 980 нм. То есть плазмонные явления в видимом и ближнем инфракрасном диапазоне в максине Ti3C2Tx происходят на длинах волн квадрупольного резонанса, т.е. на более коротких длинах волн, чем поперечные дипольные плазмоны ($\lambda \sim 1100$ нм).

3. Показано, что из-за неровностей поверхности образца генерируется поперечное электрическое поле, приводящее к возникновению поперечных плазмонов. Последние возбуждают квадрупольные колебания в максине. В димерах взаимодействующих НЧ сильный квадрупольный ПП, взаимодействующий с поперечными плазмонами на длине волны $\lambda \sim 1400$нм, вызывает резонанс Фано (деструктивную интерференцию). Эта особенность позволяет легко выбрать качественные подложки для ПУКР. Дело в том, что сильное взаимодействие в димере возможно, когда частицы расположены очень близко друг к другу, что требует высокой концентрации НЧ.

4. В случае максиновой подложки рассчитана кривая комбинационного рассеяния молекулы R6G в зависимости от размера и формы НЧ, что позволило интерпретировать известные экспериментальные результаты. Для этого сначала были рассчитаны диэлектрические функции молекул R6G и MB на основе экспериментальных данных сечения поглощения, полученных для молекулы красителя на водной или стеклянной

подложке. Поскольку диэлектрическая функция — это макроскопическое свойство, необходимое для описания оптических материалов, используемых в COMSOL, молекулы красителей моделируются как небольшие твердые сферы, поляризуемость которых известна из измерений. Моделирование проводилось с помощью численного расчета COMSOL в среде, позволяющей простой процедурой подобрать радиус небольшой сферы для соответствия экспериментальным данным по поглощению молекулами красителя. Хотя поляризация является тензорной, оптические свойства обычно усредняются по случайным ориентациям многих молекул R6G или MB. Таким образом, анизотропия поляризации не имеет значения при интерпретации экспериментов.

5. Показано, что частота рамановского сигнала слабо зависит от формы и размера НЧ Ti3C2Tx для длин волн $\lambda \leq 1000$ нм. Показана также важная роль квадрупольных резонансов в максиновых НЧ. Чтобы учесть эффект горячей точки, были исследованы взаимодействующие наноэллипсоиды и наносфероиды максина и идентифицированы особенности, возникающие в результате гибридизации ПП. В видимой-ближней инфракрасной области спектра димеры максина обеспечивают значения КУ порядка $10^5 - 10^7$, которые близки к экспериментальным данным Ti3C2Tx. Слабая зависимость КУ от размера легко синтезируемых и практически произвольной формы максиновых НЧ в видимом и ближнем инфракрасном диапазоне открывает новые возможности для использования этих подложек в традиционных приложениях ПУКР.

6. Показано, что квадрупольные ПП могут возникать в комплексах небольших наночастиц с размерами, меньшими длины волны падающего света. В частности, было показано, что эффективностью резонанса Фано можно управлять, изменяя геометрию системы малых металлических НЧ. Изменение ориентации отдельных НМ в ядре трехмерных комплексов приводит к изменению длины волны резонанса Фано. В частности, когда система частиц расположена в вершинах тетраэдра, можно изменить длину волны резонанса Фано в 2,5 раза, повернув все нижележащие частицы на 66° вокруг осей, параллельных симметрии 3-го порядка, проходящей через верхняя вершина. В этих же условиях эффективность резонанса Фано возрастает в 8 раз.